

Electrolyte Immersion Increases Photoconductivity in a Model Polymer Photocathode

William P. Kopcha,[✉] Aiswarya Abhisek Mohapatra,[✉] Casey M. Davis, Jonathan R. Thurston, Eui Hyun Suh, Bo Dong, Megan R. Brown, Aniruddha Basu, Zejie Chen, Shane Ardo, Chad M. Risko, Tianquan Lian, Erin L. Ratcliff, Stephen Barlow, Seth R. Marder, Michael F. Toney, Melissa K. Gish,* Andrew J. Ferguson,* and Obadiah G. Reid*



Cite This: *ACS Energy Lett.* 2025, 10, 4019–4026



Read Online

ACCESS |



Metrics & More

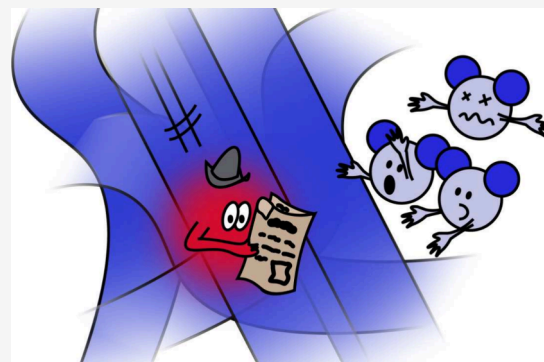


Article Recommendations



Supporting Information

ABSTRACT: Immersing polymer solar cells in aqueous electrolyte for photoelectrochemical (PEC) hydrogen production is likely to cause photophysical changes that could present both challenges and opportunities for engineering functional and durable devices. Herein we study the bulk heterojunction blend poly(4,8-bis(5-(2-ethylhexyl)thiophen-2-yl)benzo[1,2-*b*:4,5-*b'*]dithiophene-2,6-diyl)-*alt*-(2-(((2-ethylhexyl)oxy)carbonyl)-3-fluorothiopheno[3,4-*b*]thiophene-4,6-diyl):poly-(*N,N'*-di(2-octyl)dodecyl)naphthalene-1,8:4,5-bis(dicarboximide)-2,6-diyl)-*alt*-(2,2-bithiophene-5,5'-diyl) (PTB7-Th:N2200) excited-state dynamics in electrolyte from femtosecond to millisecond time scales using pump–probe microwave conductivity and absorption spectroscopy. While the blend swells very little, electrolyte exposure *increases* the microwave-frequency mobility and possibly the yield of photogenerated charges while also *decreasing* crystallinity. These results indicate an enhancement in key performance metrics, implying that any limitations on the performance of PEC test devices do not arise from active layer–electrolyte interactions. For the PTB7-Th:N2200 blend or similar photocathode systems, our results indicate that improving the interfacial kinetics and/or the carrier lifetime should be prioritized, not protecting the active layer from the electrolyte. Since this observation may not be universal to all polymer systems, future research should focus on identifying their limiting photophysical processes.



Organic semiconductors (OSCs) are promising candidates for photoelectrochemical (PEC) hydrogen production.^{1–10} PEC applications with OSCs take inspiration from the well-developed field of organic photovoltaics (OPVs). There, electron-donating and electron-accepting materials are combined in a thin-film bulk-heterojunction (BHJ) to drive photoinduced charge separation, which becomes thermodynamically favorable after the materials have absorbed a photon of the appropriate energy.^{11–15} Charges then travel via hopping transport to their ultimate destinations.^{15–17} Unlike OPVs, photoelectrochemical applications require that OSCs operate in contact with an electrolyte (often aqueous) to drive catalysis. Very little is known about how these semiconductor/electrolyte interfaces may influence photophysical behavior of OSCs.¹ In small-molecule donor–acceptor dyads in solution, changes in the solvent dielectric constant and the reorganization of the solvation shell around the excited molecules can significantly

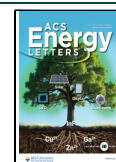
alter the thermodynamics and kinetics for charge separation and charge recombination,^{18–22} modifying the rates of these process by several orders of magnitude or, in some cases, mean the difference between achieving or not achieving a charge separated (CS) state at all. Similarly, the interface between the high dielectric-constant electrolyte and the low dielectric-constant conjugated polymer could selectively stabilize charge carriers, providing a greater opportunity for those charge carriers to perform a given function.⁶ On the other hand, the electrolyte could cause structural alterations to the complex polymer network and its different domains, be they regions of

Received: June 12, 2025

Revised: July 17, 2025

Accepted: July 18, 2025

Published: July 28, 2025



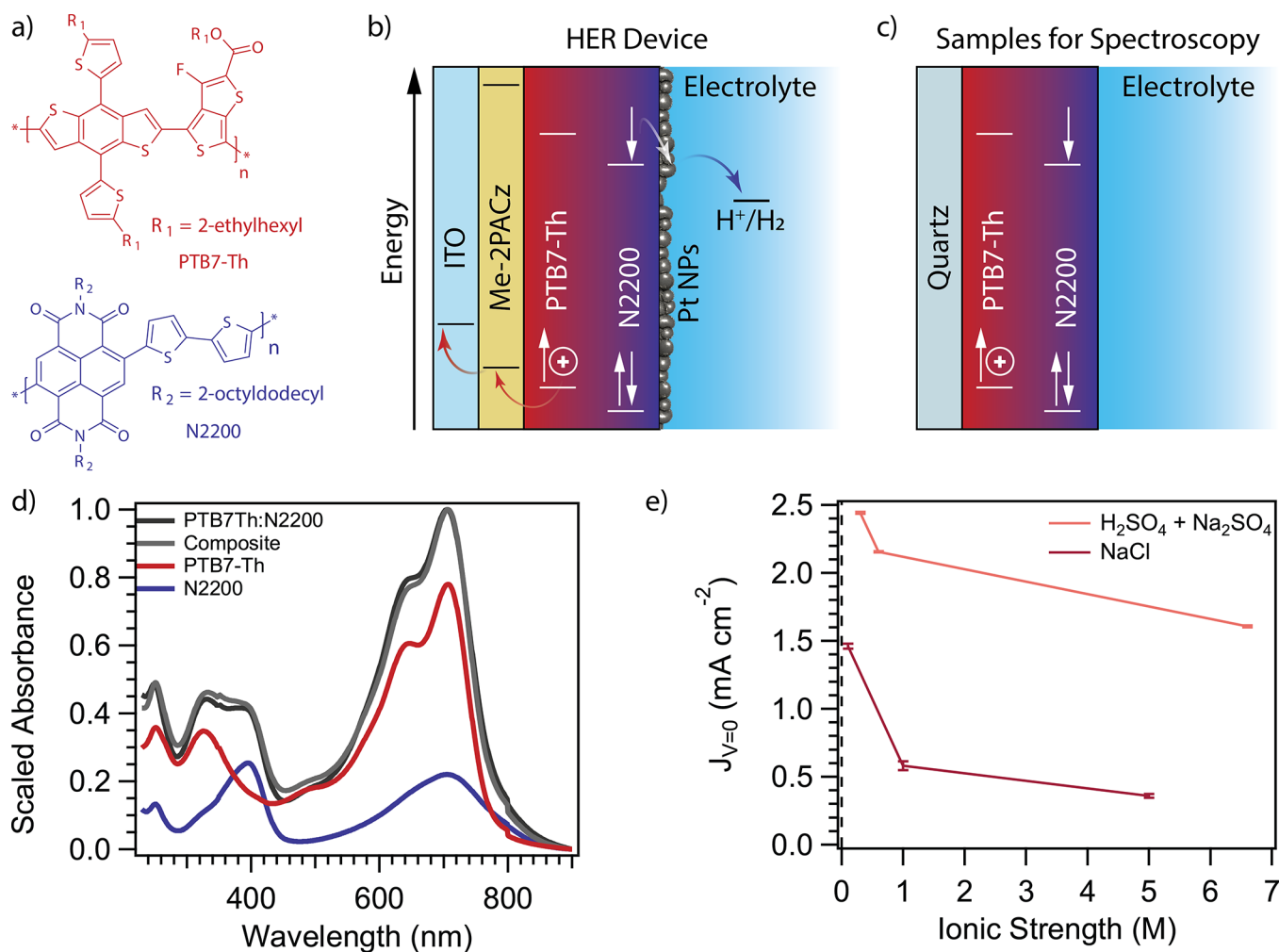


Figure 1. (a) The chemical structures of the repeat units of PTB7-Th and N2200. (b) A schematic of the device stack used in HER experiments with energy levels depicting the roles of both polymers. A photogenerated hole is created in PTB7-Th and scavenged into a hole transport layer (Me-2PACz) and ultimately the cathode, while a photogenerated electron in N2200 is transferred to a Pt cocatalyst and reduces H⁺ to H₂. (c) A schematic of the samples used for spectroscopy including only the active layer from the device stack. (d) Absorption spectra of both polymers, PTB7-Th (red) and N2200 (blue) scaled according to their contribution to the blend film, and the PTB7-Th:N2200 blend (black). A linear combination of both scaled spectra (“Composite”, gray) is included for comparison and shows excellent agreement with the measured blend film spectrum. (e) The photocurrent density at zero applied potential with respect to the reversible hydrogen electrode (RHE), a proxy for H₂ generation,³⁴ decreases as the ionic strength of the electrolyte increases. Photocurrents are plotted in the polarographic convention.

pure donor or acceptor,^{11–15} regions with varying degrees of long-range order,^{23,24} or regions with different aggregate phases.²⁵ This could disrupt an otherwise high performance BHJ structure. Factors such as these will impact optimization of the interface between the semiconductor, catalyst, and electrolyte to best utilize the photogenerated charges within the active layer.

To explore the issues noted above, we examine the changes in photophysical behavior of polymer:polymer BHJ blend formed from poly(4,8-bis(5-(2-ethylhexyl)thiophen-2-yl)benzo[1,2-*b*:4,5-*b'*]dithiophene-2,6-diyl)-*alt*-(2-((2-ethylhexyl)oxy)carbonyl)-3-fluorothiopheno[3,4-*b*]thiophene-4,6-diyl) and poly(*N,N'*-di(2-octyldodecyl)naphthalene-1,8:4,5-bis(dicarboximide)-2,6-diyl)-*alt*-(2,2-bithiophene-5,5'-diyl) (PTB7-Th:N2200) through exposure to electrolyte environments. We test the hypothesis stated above: the polymer:electrolyte interface or “interphase” can stabilize charges, extending this to include the influence of salt concentration. Salts have sometimes been shown to improve hydrogen

evolution reaction (HER) performance through Coulombic stabilization of charge carriers,^{26–28} though exposure to water can have deleterious effects on some OPV materials.^{29–31} As noted previously, producing and stabilizing photogenerated charges to be harvested is but one step in this complex process. In testing this hypothesis, we focus on related subquestions to elucidate this step: how permeable is a nominally hydrophobic film^{32,33} to the aqueous electrolyte with which it is in direct contact? Is the microstructure of the BHJ significantly perturbed?

We find that the GHz-frequency charge carrier mobility and possibly also the charge carrier yield in a PTB7-Th:N2200 (2:1 w/w) BHJ blend *increase* in the presence of aqueous electrolyte, driven primarily by an antisolvent annealing effect that *reduces* the crystallinity of the film. Changes to the dynamics from femtoseconds to milliseconds are accompanied by drastic changes to the structure, as shown by X-ray scattering, but with very little water uptake. The trends in HER performance in test devices do not reflect the enhancement of

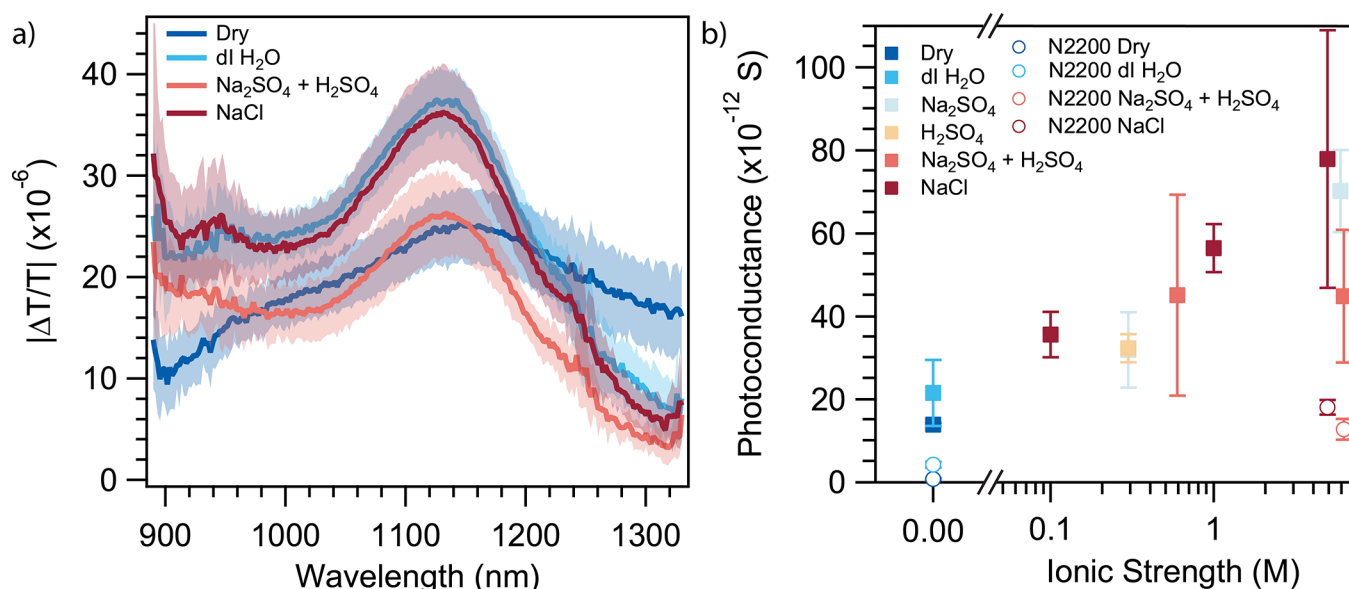


Figure 2. (a) Photomodulation spectra of the blend film taken in various electrolyte environments at a modulation frequency of 10 kHz and 1.1×10^{17} absorbed photons/cm²/s ($\lambda_{\text{exc}} = 640$ nm). The total signal magnitude (R) was used as a measure of polaron yield. (b) A summary of the SSMC photoconductance data for the blend film in various electrolyte environments (filled symbols) measured at 10 kHz modulation frequency and 5×10^{16} absorbed photons/cm²/s (broadband white-light source (400–800 nm)). Note that a neat N2200 film was used to act as a control for the dielectric response of the electrolyte (empty symbols).

photogenerated charge carrier yield and mobility in the active layer. This observation underscores the fact that charge generation and transport are but the first steps in a complex process leading from photon absorption to hydrogen evolution. We thus conclude that the model PTB7-Th:N2200 BHJ studied here is fundamentally suitable for PEC applications from a photophysical durability standpoint and the performance of the HER devices may well be limited by steps further down the photochemical pathway, possibly including macroscopic mass transport, charge access to the electrochemically active interface, or interfacial kinetics for hole extraction or hydrogen evolution.

Figure 1 shows the structures and absorbance spectra of the polymers used in this study, as well as the construction of the PEC half-cell and samples for spectroscopic measurements, and the magnitude of the photocurrent density at zero applied potential vs the reversible hydrogen electrode (RHE) (see Sections S1.2 and S1.3 for a detailed description of the PEC device construction, Section S3.4 for details on the HER experiments, and S3.14, including Figures S47 and S48, for further discussion on the impact of Pt nanoparticles on the charge dynamics). A blend of PTB7-Th:N2200 in a 2:1 weight ratio was used as the BHJ active layer (see Figure 1d for the blend's absorption spectrum, as well as Figure S13) with platinum nanoparticles deposited as a surface cocatalyst and solutions of either Na₂SO₄ and H₂SO₄, which is typical for the HER reaction, or NaCl, which has a high solubility in water, enabling study of highly concentrated electrolyte. The photocurrent densities at zero potential with respect to the reversible hydrogen electrode (RHE) of ~ 2 mA/cm² we measure here are only 15–20% of the 10–15 mA/cm² typical of comparable OPV devices³⁵ and optimized inorganic PEC cells.³⁶ Moreover, we find that the photocurrent density declines with increasing salt concentration, contrary to a recent motivating report on a different photocathode,²⁶ and contrary to our base hypothesis that solvation or ion pairing of charges

in the conjugated polymer with the electrolyte solution could stabilize carriers and enhance hydrogen evolution.

Thus, we investigated the polymer active layer, since photogenerated charge carrier density in it governs the reduction of H⁺ to H₂. We performed a detailed series of spectroscopic experiments spanning from the femtosecond to millisecond time scales in order to discover whether the observed trends in photocurrent density are caused by changes in the ability of the active layer to maintain a sufficient concentration of photogenerated charge, or if they are instead limited by device-level phenomena such as the transport of charges to the electrochemically active interfaces, deleterious interfacial trap states, or the rate of interfacial proton reduction.

Combining steady-state photoinduced absorption (SSPIA)³⁷ and steady-state microwave conductivity (SSMC)^{38,39} methods allows us to separate trends in charge carrier concentration and mobility on the millisecond time scale relevant to the catalytic process. SSPIA (see Section S1.11, Figure S6 for a detailed description of SSPIA and the control experiments performed) provides information about the charge concentration via Beer's Law, assuming a near-constant extinction coefficient of charges, while SSMC gives a carrier concentration-mobility product via photoconductance. Figure 2a shows a near-infrared SSPIA spectrum for four different environmental conditions of the same PTB7-Th:N2200 film. Notably, the peaks that we see are identical to those observed in our transient absorption (TA) data (*vide infra*, notably Figure 3b), and in published TA and spectroelectrochemistry data.^{24,40–42} We therefore assign the photoinduced absorption (PIA) with a λ_{max} between 1100 and 1200 nm to the PTB7-Th positive polaron and the shoulder around 900 nm to the polarons in both polymers (see Section S3.13, particularly Figure S37). We used the same acidic (Na₂SO₄ with H₂SO₄) and neutral (NaCl alone) media as in the HER experiments to enable direct comparisons. The increase in the PTB7-Th positive polaron PIA peak height between the dry and electrolyte immersed film indicates a

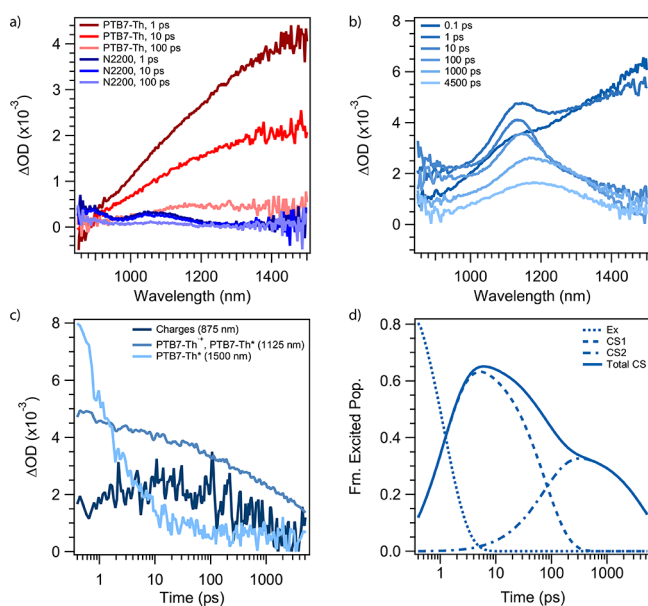


Figure 3. (a) Transient absorption spectra of the neat polymer films, PTB7-Th (red) and N2200 (blue), at several delay times. Note these are two separate experiments done under the same conditions ($\lambda_{\text{pump}} = 600$ nm, 40 nJ/pulse or $\sim 2.6 \times 10^{18}$ photons/cm²) and all spectra are shown on the same ΔOD scale. (b) Transient absorption spectra of the blend film showing rapid evolution from the PTB7-Th exciton to a new feature centered between 1100 and 1150 nm, which we attribute to the PTB7-Th cation. The feature between 800 and 900 nm contains contributions from the charged states of both polymers. (c) Transient absorption kinetic traces of the blend film showing concomitant decay of the PTB7-Th exciton and the rise of charged states in both polymers, as well as their decay on the several-ns time scale. (d) The results of global fitting of the transient absorption data for the blend film showing the evolution of the populations of the PTB7-Th exciton (Ex), two spectrally distinct charge-separated (CS) states, and the sum total of both CS states over time as a fraction of the number of absorbed photons.

modest increase of up to 43% at the 10 kHz modulation frequency used in these experiments. Section S3.9 of the Supporting Information, especially Figure S26, details the determination of upper (43%) and lower (0%) bounds using the PIA data.

For comparison, Figure 2b shows the trends in photoconductance measured by SSMC on identical PTB7-Th:N2200 blend films upon exposure to electrolyte. These data show up to a 4-fold increase under the same conditions. Using the 0–43% charge yield from SSPIA, this translates to an increase in the AC GHz-frequency mobility of ~ 2.8 – $4\times$. Control SSMC experiments with N2200 films (Figure 2a), which do not readily generate large charge carrier densities,^{41,43} were performed to rule out interference from thermal artifacts (see Sections S1.7 and S1.8, Figures S4 and S5).⁴⁴ SSPIA cannot distinguish between bound and free charges, whereas SSMC is only sensitive to free mobile charges. Immersion in aqueous electrolyte could be shifting the fraction of bound vs free charges,⁴⁵ thus increasing the average measured mobility. These are not distinguishable possibilities with the present data, and we conclude that at steady-state, the concentration of photogenerated charges and their average GHz frequency mobility both appear to increase when PTB7-Th:N2200 blend films are submerged in aqueous electrolyte

with increasing salt concentration, providing a stark contrast to the modest HER performance observed with the whole device, which decreases with increasing electrolyte concentration. We proceeded to investigate the origins of the observed effects, particularly with regard to the possible increase in charge yield, with ultrafast spectroscopic techniques.

Figure 3a shows pertinent spectral features probed by fs-ps TA of the neat polymer films in the NIR after photoexcitation at 600 nm. The signal of the PTB7-Th exciton dominates compared to the N2200 exciton, which absorbs weakly at this wavelength (Figure 1d). Figure 3b shows the TA spectrum of the blend film as it evolves over time. The spectrum at 0.1 ps closely resembles the neat PTB7-Th exciton. Over the next few ps, new PIAs appear at wavelengths <900 nm and centered around 1125 nm, which based on previous literature reports^{24,40–42} correspond to charged states in both polymers (<900 nm) and the PTB7-Th radical cation (1125 nm). The PIA of the PTB7-Th radical cation redshifts and broadens over time as the hole migrates to lower-energy regions of the polymer (see Figures S35–S37 for the complete TA spectra for all tested conditions). Figure 3c shows the kinetics at key wavelengths, showing that charge separation is complete by ~ 5 ps. Since the spectral features associated with the different excited state species are rather broad and overlap, we performed global fitting⁴⁶ of the two-dimensional TA data to extract population dynamics. See Section S3.13, Figures S38–S46, and Tables S8 and S9 for a detailed discussion. Figure 3d shows the results of the global fit in terms of the evolution of the population of states over time as a fraction of the number of absorbed photons. Based on the rate constants connecting the Ex to CS₁ (5.7×10^{11} s⁻¹), CS₁ to CS₂ (6.8×10^9 s⁻¹), and each of these states to the ground state (GS; 2.8×10^{11} s⁻¹, 6.4×10^9 s⁻¹, and 1.9×10^8 s⁻¹, respectively), the global fitting estimates residual charge at 5 ns corresponding to approximately $\sim 14\%$ of the absorbed photons.

The blend films in aqueous environments all showed slower decay of the PTB7-Th radical cation peak than the dry blend film in fs-ps TA measurements (Figure 4c), indicating that an aqueous environment leads to greater residual charge on the ns time scale. This is consistent with the SSPIA/SSMC data and is corroborated by the observed increase in the initial ($t = 0$) yield-mobility product ($\phi\Sigma\mu$) from time-resolved microwave conductivity (TRMC) measurements in the same environments (Figure 4; see Section S3.7, Figures S19–S24 for a description of the measurements and control experiments performed). The fact that the trend in the initial $\phi\Sigma\mu$ from the TRMC, with an instrument response function (IRF) of roughly 10 ns, tracks well with the trend in residual PTB7-Th cation signal at the maximum delay time for our TA instrument (5.3 ns) suggests that more photogenerated charges survive into the ns time scale in the films exposed to an aqueous environment. Global fitting of the TA data for all conditions supports this, estimating 19% charge retention for the solution in 5 M NaCl, 16% in 0.1 M Na₂SO₄ and 0.1 M H₂SO₄, and 18% in water, compared to 14% in the dry film at 5 ns (see Section S3.13, Figures S38–S46, and Tables S8 and S9 for a detailed discussion of the global fitting process). If the SSPIA measurements (Figure 1b) indeed indicate greater charge yield for films in aqueous environments, it is likely due to the slower recombination observed on the ps-ns time scale, leading to the higher residual charge concentration.

The blend films in aqueous media also have higher amounts of charge at very early times (Figure 4b: 1 ps spectra) as

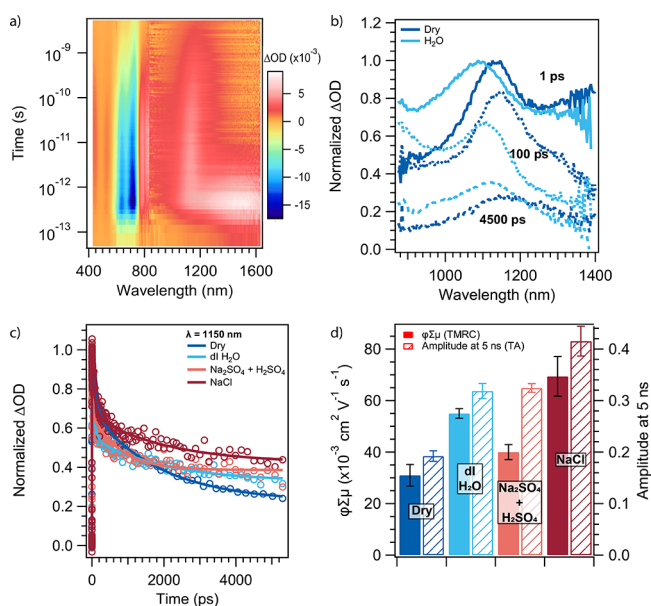


Figure 4. (a) A representative two-dimensional map of the transient absorption data of the dry blend film spanning the visible and NIR regions of the spectrum ($\lambda_{exc} = 600$ nm, 40 nJ/pulse). The other conditions can be found in Figures S42, S44, and S46. (b) A comparison of the evolution of the spectra of the dry blend film and the blend film soaked in water. Note the higher peak at 900 nm corresponding to charges at 1 ps, the lack of a shoulder at 1300 nm at 100 ps, and the larger residual peak at 4500 ps in the film exposed to water. (c) Kinetic traces of the blend film in various electrolyte environments tracking the decay of the PTB7-Th cation at 1150 nm. The $\text{Na}_2\text{SO}_4 + \text{H}_2\text{SO}_4$ solution is 0.1 M in each component, while the NaCl solution is 5 M. (d) A comparison of the initial yield-mobility product (solid bars) from TRMC measurements and residual peak amplitude at 5 ns of the PTB7-Th cation from TA measurements (striped bars) of the blend film for various electrolyte environments. The concentrations are the same as in (c).

indicated by the higher relative absorbance in the 800–900 nm region. Additionally, spectral differences between dry and aqueous conditions suggest morphological changes in the polymer via the disappearance of a shoulder at 1300 nm, blueshifting of the PTB7-Th positive polaron (Figure 4b: 100 ps spectra, Sections S3.10–S3.12, Figures S30–S34, and Tables S6 and S7), and narrowing of peaks (Figure 4b: 100 and 4500 ps spectra). We therefore performed a series of X-ray characterization measurements on both dry blend films and blends soaked in water to evaluate the nature of any structural changes.

We performed X-ray reflectivity (XRR) and grazing-incidence wide-angle X-ray scattering (GIWAXS) measurements on the polymer BHJ film to gain insight into the structural changes induced in the film by aqueous media (see Section S1.12 for a detailed discussion of XRR and Section S1.13 for a detailed discussion of GIWAXS). Figure S10 shows the results of GIWAXS measurements of films soaked in electrolyte taken *ex-situ* under vacuum. They show a decrease in signal intensity of roughly two-thirds upon soaking and drying. Such a sizable decrease clearly indicates increased disorder in the soaked films, as only ordered regions are able to diffract X-rays. The differences in intensity cannot be explained by differences in thickness, which were within 10% of each other according to profilometry measurements (see Table S2).

Additionally, for the film exposed to aqueous media there is a slight peak shift to lower q of the $\sim 0.4 \text{ \AA}^{-1}$ diffraction feature, indicating a small increase in the interlamellar spacing. Intriguingly, *in situ* XRR measurements (Section S1.12, Figure S8) show an increase in film thickness of only $\sim 2.3\%$ for a sample measured in a chamber held at 94% relative humidity after soaking in water. Though a more complicated relationship between the electrolyte identity, concentration, and structural reorganization likely exists (see Figures 2b, S10b, S20–S24), it is beyond the scope of this investigation. The most impactful factor, though, is simply exposure to water, which is not absorbed into the film in significant quantities.

A consistent picture emerges when considering the totality of the data: The yield and GHz-frequency mobility of charges increase upon exposure of the BHJ film to aqueous media. The amount of solvent taken up by the films is small, as shown by XRR and complementary FTIR measurements, the latter showing no measurable OH stretching peaks in a film soaked for an hour in water (see Section S3.3, Figure S15). Accordingly, any change to ΔG of charge separation or recombination is expected to be small—roughly 100 meV (see Section S3.8, Figure S25 for further discussion). We find the sizable structural changes to be a more compelling explanation than the small change in driving force for the observations shown here. GIWAXS reveals a definite decrease in long-range order, with the scattering intensity decreasing by about two-thirds between the dry samples and those exposed to an aqueous medium. We propose that the primary driver of photophysical changes in PTB7-Th:N2200 blends upon electrolyte immersion is an antisolvent annealing effect that drives polymer chain reorganization, propagating from the polymer–water interface to minimize the energetic penalty of the hydrophobic polymer being in contact with water. The increase in the GHz-frequency mobility of the films combined with the loss of structural order seen in GIWAXS strongly suggest that we are observing the *intra-chain* mobility of charges increase as chain–chain contacts decrease. This is consistent with prior studies that have shown similar contributions to thin-film mobilities from inter- and intrachain components, and the general observation that extended polymer chains in solution usually present much larger microwave-frequency mobilities than the corresponding thin-films.^{47–50}

While it is possible to view the photophysics through the lens of Marcus charge-transfer kinetics, it is likely that the recombination rate constants we observe are connected with diffusional re-encounter of electron hole pairs, not the fundamental rate constant of a charge-transfer state recombining. Nonetheless, we include such an analysis in Section S3.8; see particularly Figure S25 and Tables S3–S5.

It is important to emphasize that no deleterious effects on the photophysics of the active layer were seen from simply exposing it to electrolyte. The polymer active layer shows no change in absorbance by UV–vis–NIR spectrophotometry after HER testing (Figure S18) and has therefore not degraded, as this would cause photobleaching of the intramolecular charge-transfer band at ~ 700 nm.⁵¹ The device stability shown in Figures S17 and S18 reinforces this. Figure S17 shows that the SSPIA and SSMC signals are reduced by 10–20% over the course of an hour of continuous illumination as long as oxygen is excluded, indicating minimal degradation. The chronoamperometry data performed under HER conditions shows an initial drop in current (Figure S17), possibly

due to the formation of hydrogen bubbles that cover the electrode, preventing large portions from contacting the electrolyte.^{52–54} Surface trap states on the ITO, depletion of H⁺ in the vicinity of the electrode, and transient capacitive current from turning on the light source may also contribute to the photocurrent reduction (see Section S3.5 for more discussion).

We have shown that the presence of aqueous electrolyte enhances key metrics such as the GHz-frequency mobility and the nanosecond charge yield in the model donor–acceptor polymer blend PTB7-Th:N2200; it is not detrimental to the photoinitiated charge generation step in the HER process. Antisolvent annealing causes structural changes in the polymers when exposed to an aqueous environment, leading to the increased yield and *intrachain* charge carrier mobility. As a result, charges separate more quickly and recombine more slowly, though at this time it is hard to establish with certainty the mechanistic origin of this effect and how it is induced by these structural changes. The operation of a whole device involves more than simply generating charges in the active layer: generated electrons must interact with H⁺ at the surface of a cocatalyst. Thus, the charge carrier lifetimes must be commensurate with mass transport of the H⁺ to the cocatalyst. Meanwhile, holes must be transported through the polymer network and hole-transport layer (HTL) into the ITO (see Figure 1). They may be impeded from doing so by, e.g., interfacial trap states. This is not to say that PTB7-Th:N2200 is already an optimal photocathode material for PEC generation of hydrogen—only that electrolyte exposure does not make it worse, and researchers should look elsewhere to understand why HER photocurrent densities are relatively low compared to corresponding OPV devices. Thus, in addition to further optimization of charge generation and lifetime for these and similar polymers, other factors, such as the impact of the solution composition on mass transport, alterations of interfacial behaviors, changes in hydrophilicity, porosity, and surface area, etc. are prime candidates for further study in improving photoelectrochemically driven reactions in OSCs.

■ ASSOCIATED CONTENT

SI Supporting Information

The Supporting Information is available free of charge at <https://pubs.acs.org/doi/10.1021/acsenergylett.5c01809>.

Instrumentation, sample preparation, control experiments related to residual palladium and atmospheric oxygen, characterization by profilometry and optical absorbance, water detection in soaked films by FTIR, XRR, GIWAXS, HER chronoamperometry, stability testing of films under illumination, additional discussion of Marcus theory and its application to CT states, additional discussion of microwave spectroscopies including control experiments to check for thermal artifacts and changes to cavity K factor when working with aqueous samples, additional discussion of SSPIA measurements including phase correction and real vs imaginary parts of the signal, computational chemistry methods and TDDFT results, triplet sensitization experimental conditions and results, and additional discussion of TA spectral features, TA global fitting methods and results, and TA on films with vs without Pt nanoparticles (PDF)

■ AUTHOR INFORMATION

Corresponding Authors

Melissa K. Gish – Materials, Chemical, and Computational Science Directorate, National Renewable Energy Laboratory, Golden, Colorado 80401, United States; orcid.org/0000-0002-9886-3626; Email: melissa.gish@nrel.gov

Andrew J. Ferguson – Materials, Chemical, and Computational Science Directorate, National Renewable Energy Laboratory, Golden, Colorado 80401, United States; orcid.org/0000-0003-2544-1753; Email: andrew.ferguson@nrel.gov

Obadiah G. Reid – Materials, Chemical, and Computational Science Directorate, National Renewable Energy Laboratory, Golden, Colorado 80401, United States; Renewable and Sustainable Energy Institute, University of Colorado Boulder, Boulder, Colorado 80309, United States; orcid.org/0000-0003-0646-3981; Email: obadiah.reid@colorado.edu

Authors

William P. Kopcha – Materials, Chemical, and Computational Science Directorate, National Renewable Energy Laboratory, Golden, Colorado 80401, United States; orcid.org/0000-0001-8811-1669

Aiswarya Abhisek Mohapatra – Renewable and Sustainable Energy Institute, University of Colorado Boulder, Boulder, Colorado 80309, United States; orcid.org/0000-0002-4633-7771

Casey M. Davis – Department of Chemistry, University of Colorado Boulder, Boulder, Colorado 80309, United States; orcid.org/0000-0001-9167-5772

Jonathan R. Thurston – Department of Chemistry, University of Colorado Boulder, Boulder, Colorado 80309, United States; orcid.org/0000-0003-1275-8823

Eui Hyun Suh – School of Materials Science and Engineering, Georgia Institute of Technology, Atlanta, Georgia 30332, United States

Bo Dong – Department of Chemistry, Emory University, Atlanta, Georgia 30332, United States

Megan R. Brown – Department of Chemistry, University of Kentucky, Lexington, Kentucky 40506, United States

Aniruddha Basu – Renewable and Sustainable Energy Institute, University of Colorado Boulder, Boulder, Colorado 80309, United States

Zejie Chen – Department of Chemistry, University of California Irvine, Irvine, California 92697, United States

Shane Ardo – Department of Chemistry, Department of Chemical and Biomolecular Engineering, and Department of Materials Science and Engineering, University of California Irvine, Irvine, California 92697, United States; orcid.org/0000-0001-7162-6826

Chad M. Risko – Department of Chemistry, University of Kentucky, Lexington, Kentucky 40506, United States; orcid.org/0000-0001-9838-5233

Tianquan Lian – Department of Chemistry, Emory University, Atlanta, Georgia 30332, United States; orcid.org/0000-0002-8351-3690

Erin L. Ratcliff – School of Materials Science and Engineering, Georgia Institute of Technology, Atlanta, Georgia 30332, United States; orcid.org/0000-0002-2360-8436

Stephen Barlow – Renewable and Sustainable Energy Institute, University of Colorado Boulder, Boulder, Colorado 80309, United States; Materials, Chemical, and Computational Science Directorate, National Renewable

Energy Laboratory, Golden, Colorado 80401, United States;

orcid.org/0000-0001-9059-9974

Seth R. Marder – Renewable and Sustainable Energy Institute, Department of Chemistry, Department of Chemical and Biological Engineering, and Materials Science and Engineering Program, University of Colorado Boulder, Boulder, Colorado 80309, United States; Materials, Chemical, and Computational Science Directorate, National Renewable Energy Laboratory, Golden, Colorado 80401, United States

Michael F. Toney – Renewable and Sustainable Energy Institute, Department of Chemical and Biological Engineering, and Materials Science and Engineering Program, University of Colorado Boulder, Boulder, Colorado 80309, United States; orcid.org/0000-0002-7513-1166

Complete contact information is available at:

<https://pubs.acs.org/10.1021/acsenenergylett.5c01809>

Author Contributions

W.P.K. and A.A.M. contributed equally to this work.

Notes

The authors declare no competing financial interest.

ACKNOWLEDGMENTS

This work was authored in part by the National Renewable Energy Laboratory for the U.S. Department of Energy (DOE) under Contract No. DE-AC36-08GO28308. This work was primarily performed by the Center for Soft PhotoElectro-Chemical Systems (SPECS) Energy Frontier Research Center, award DE-SC0023411, unless otherwise noted below, with funding provided by the U.S. Department of Energy, Division of Chemical Sciences, Geosciences, and Biosciences, Office of Basic Energy Sciences. The views expressed in the article do not necessarily represent the views of the DOE or the U.S. Government. S.A. and Z.C. acknowledge support for initial conception and testing of TRMC methods on semiconductor/liquid interfaces as part of Ensembles of Photosynthetic Nanoreactors (EPN), an Energy Frontier Research Center funded by the United States Department of Energy, Office of Science under Award Number DE-SC0023431. We thank Dragan Mejic, University of Colorado - Boulder Chemical and Biological Engineering Instrument Shop Supervisor, for his assistance with designing and machining of the XRR cell. This research was supported in part by the Colorado Shared Instrumentation in Nanofabrication and Characterization (COSINC): the COSINC-CHR (RRID: SCR_018985), College of Engineering & Applied Science, University of Colorado Boulder, for operation of the X-ray diffraction instrument with which the X-ray reflectivity measurements were taken. The authors would like to acknowledge the support of the staff and the facilities that have made this work possible. We thank David T. Moore and Ross A. Kerner for their performance of ICP-MS measurements and analysis to quantify the adventitious Pd content of our polymers.

REFERENCES

- (1) Ratcliff, E. L.; Chen, Z.; Davis, C. M.; Suh, E. H.; Toney, M. F.; Armstrong, N. R.; Reid, O. G.; Greenaway, A. L. Soft Materials for Photoelectrochemical Fuel Production. *ACS Energy Letters* **2023**, *8*, 5116–5127.
- (2) O'Connor, M. M.; Aubry, T. J.; Reid, O. G.; Rumbles, G. Charge Concentration Limits the Hydrogen Evolution Rate in Organic Nanoparticle Photocatalysts. *Adv. Mater.* **2024**, *36*, 2210481.

- (3) Sachs, M.; Sprick, R. S.; Pearce, D.; Hillman, S. A. J.; Monti, A.; Guilbert, A. A. Y.; Brownbill, N. J.; Dimitrov, S.; Shi, X.; Blanc, F.; Zwiijnenburg, M. A.; Nelson, J.; Durrant, J. R.; Cooper, A. I. Understanding structure-activity relationships in linear polymer photocatalysts for hydrogen evolution. *Nat. Commun.* **2018**, *9*, 4968.
- (4) Kosco, J.; et al. Enhanced photocatalytic hydrogen evolution from organic semiconductor heterojunction nanoparticles. *Nat. Mater.* **2020**, *19*, 559–565.
- (5) Sprick, R. S.; Little, M. A.; Cooper, A. I. Organic heterojunctions for direct solar fuel generation. *Communications Chemistry* **2020**, *3*, 40.
- (6) Hillman, S. A. J.; Sprick, R. S.; Pearce, D.; Woods, D. J.; Sit, W.-Y.; Shi, X.; Cooper, A. I.; Durrant, J. R.; Nelson, J. Why Do Sulfone-Containing Polymer Photocatalysts Work So Well for Sacrificial Hydrogen Evolution from Water? *J. Am. Chem. Soc.* **2022**, *144*, 19382–19395.
- (7) Yang, C.; Ma, B. C.; Zhang, L.; Lin, S.; Ghasimi, S.; Landfester, K.; Zhang, K. A. I.; Wang, X. Molecular Engineering of Conjugated Polybenzothiadiazoles for Enhanced Hydrogen Production by Photosynthesis. *Angew. Chem., Int. Ed.* **2016**, *55*, 9202–9206.
- (8) Wang, L.; Fernández-Terán, R.; Zhang, L.; Fernandes, D. L. A.; Tian, L.; Chen, H.; Tian, H. Organic Polymer Dots as Photocatalysts for Visible Light-Driven Hydrogen Generation. *Angew. Chem., Int. Ed.* **2016**, *55*, 12306–12310.
- (9) Sprick, R. S.; Bonillo, B.; Clowes, R.; Guiglion, P.; Brownbill, N. J.; Slater, B. J.; Blanc, F.; Zwiijnenburg, M. A.; Adams, D. J.; Cooper, A. I. Visible-Light-Driven Hydrogen Evolution Using Planarized Conjugated Polymer Photocatalysts. *Angew. Chem., Int. Ed.* **2016**, *55*, 1792–1796.
- (10) Borno, P.; Prévot, M. S.; Yu, X.; Guijarro, N.; Sivula, K. Direct Light-Driven Water Oxidation by a Ladder-Type Conjugated Polymer Photoanode. *J. Am. Chem. Soc.* **2015**, *137*, 15338–15341.
- (11) Mazzio, K. A.; Luscombe, C. K. The future of organic photovoltaics. *Chem. Soc. Rev.* **2015**, *44*, 78–90.
- (12) Kippelen, B.; Brédas, J.-L. Organic photovoltaics. *Energy Environ. Sci.* **2009**, *2*, 251–261.
- (13) Zhang, G.; Lin, F. R.; Qi, F.; Heumüller, T.; Distler, A.; Egelhaaf, H.-J.; Li, N.; Chow, P. C. Y.; Brabec, C. J.; Jen, A. K.-Y.; Yip, H.-L. Renewed Prospects for Organic Photovoltaics. *Chem. Rev.* **2022**, *122*, 14180–14274.
- (14) Sampaio, P. G. V.; González, M. O. A. A review on organic photovoltaic cell. *International Journal of Energy Research* **2022**, *46*, 17813–17828.
- (15) Ostroverkhova, O. Organic Optoelectronic Materials: Mechanisms and Applications. *Chem. Rev.* **2016**, *116*, 13279–13412.
- (16) Coropceanu, V.; Cornil, J.; da Silva Filho, D. A.; Olivier, Y.; Silbey, R.; Brédas, J.-L. Charge Transport in Organic Semiconductors. *Chem. Rev.* **2007**, *107*, 926–952.
- (17) Bäessler, H.; Köhler, A. In *Unimolecular and Supramolecular Electronics I: Chemistry and Physics Meet at Metal-Molecule Interfaces*; Metzger, R. M., Ed.; Springer Berlin Heidelberg: Berlin, Heidelberg, 2012; pp 1–65.
- (18) Turro, N. J.; Ramamurthy, V.; Scaiano, J. C. *Modern Molecular Photochemistry of Organic Molecules*; University Science Books: Melville, NY, 2010.
- (19) Kuciauskas, D.; Liddell, P. A.; Lin, S.; Stone, S. G.; Moore, A. L.; Moore, T. A.; Gust, D. Photoinduced Electron Transfer in CarotenoporphyrrinFullerene Triads: Temperature and Solvent Effects. *J. Phys. Chem. B* **2000**, *104*, 4307–4321.
- (20) Zieleniewska, A.; Lodemeyer, F.; Roth, A.; Guldi, D. M. Fullerenes – how 25 years of charge transfer chemistry have shaped our understanding of (interfacial) interactions. *Chem. Soc. Rev.* **2018**, *47*, 702–714.
- (21) Hou, Y.; Zhang, X.; Chen, K.; Liu, D.; Wang, Z.; Liu, Q.; Zhao, J.; Barbon, A. Charge separation, charge recombination, long-lived charge transfer state formation and intersystem crossing in organic electron donor/acceptor dyads. *Journal of Materials Chemistry C* **2019**, *7*, 12048–12074.
- (22) Kaur, R.; Possanza, F.; Limosani, F.; Bauroth, S.; Zannoni, R.; Clark, T.; Arrigoni, G.; Tagliatesta, P.; Guldi, D. M. Understanding

and Controlling Short- and Long-Range Electron/Charge-Transfer Processes in Electron Donor–Acceptor Conjugates. *J. Am. Chem. Soc.* **2020**, *142*, 7898–7911.

(23) Clark, J.; Silva, C.; Friend, R. H.; Spano, F. C. Role of Intermolecular Coupling in the Photophysics of Disordered Organic Semiconductors: Aggregate Emission in Regioregular Polythiophene. *Phys. Rev. Lett.* **2007**, *98*, 206406.

(24) Trefz, D.; Ruff, A.; Tkachov, R.; Wieland, M.; Goll, M.; Kiriya, A.; Ludwigs, S. Electrochemical Investigations of the N-Type Semiconducting Polymer P(NDI2OD-T2) and Its Monomer: New Insights in the Reduction Behavior. *J. Phys. Chem. C* **2015**, *119*, 22760–22771.

(25) Karunasena, C.; Thurston, J. R.; Chaney, T. P.; Li, H.; Risko, C.; Coropceanu, V.; Toney, M. F.; Bredas, J.-L. Polymorphs of the n-Type Polymer P(NDI2OD-T2): A Comprehensive Description of the Impact of Processing on Crystalline Morphology and Charge Transport. *Adv. Funct. Mater.* **2025**, *35*, 2422156.

(26) Li, Y.; Zhou, H.; Cai, S.; Prabhakaran, D.; Niu, W.; Large, A.; Held, G.; Taylor, R. A.; Wu, X.-P.; Tsang, S. C. E. Electrolyte-assisted polarization leading to enhanced charge separation and solar-to-hydrogen conversion efficiency of seawater splitting. *Nature Catalysis* **2024**, *7*, 77–88.

(27) Jiang, L.; Luan, J.; Zhang, H.; Bai, Y.; Zhang, Y.; Liu, W.; Yan, Z.; Zhao, H. Interference mechanism of electrolyte cations on vanadium-oxygen binary doped carbon nitride for hydrogen evolution from artificial seawater splitting: Coupling experiments, DFT calculations and machine learning. *Applied Catalysis B: Environment and Energy* **2025**, *362*, 124781.

(28) Dingenen, F.; Verbruggen, S. W. Tapping hydrogen fuel from the ocean: A review on photocatalytic, photoelectrochemical and electrolytic splitting of seawater. *Renewable and Sustainable Energy Reviews* **2021**, *142*, 110866.

(29) Yin, H.; Yan, J.; Ho, J. K. W.; Liu, D.; Bi, P.; Ho, C. H. Y.; Hao, X.; Hou, J.; Li, G.; So, S. K. Observing electron transport and percolation in selected bulk heterojunctions bearing fullerene derivatives, non-fullerene small molecules, and polymeric acceptors. *Nano Energy* **2019**, *64*, 103950.

(30) Yang, Q. D.; Ng, T.-W.; Lo, M.-F.; Wang, F. Y.; Wong, N. B.; Lee, C.-S. Effect of Water and Oxygen on the Electronic Structure of the Organic Photovoltaic. *J. Phys. Chem. C* **2012**, *116*, 10982–10985.

(31) Dang, V.-H.; Nguyen, T.-A.; Le, M.-V.; Nguyen, D. Q.; Wang, Y. H.; Wu, J. C.-S. Photocatalytic hydrogen production from seawater splitting: Current status, challenges, strategies and prospective applications. *Chemical Engineering Journal* **2024**, *484*, 149213.

(32) Kim, J. Y.; Jarka, P.; Hajduk, B.; Bednarski, H.; Szeluga, U.; Tański, T. Phase behavior of α -conjugated polymer and non-fullerene acceptor (PTB7-Th:ITIC) solutions and blends. *Sci. Rep.* **2022**, *12*, 20849.

(33) Ren, C.; He, Y.; Li, S.; Sun, Q.; Liu, Y.; Wu, Y.; Cui, Y.; Li, Z.; Wang, H.; Hao, Y.; Wu, Y. Double electron transport layers for efficient and stable organic-inorganic hybrid perovskite solar cells. *Org. Electron.* **2019**, *70*, 292–299.

(34) Chen, Z.; Dinh, H. N.; Miller, E. *Photoelectrochemical Water Splitting*; SpringerBriefs in Energy; Springer: New York, 2013.

(35) Lee, W.; Lee, C.; Yu, H.; Kim, D.-J.; Wang, C.; Woo, H. Y.; Oh, J. H.; Kim, B. J. Side Chain Optimization of Naphthalenediimide–Bithiophene-Based Polymers to Enhance the Electron Mobility and the Performance in All-Polymer Solar Cells. *Adv. Funct. Mater.* **2016**, *26*, 1543–1553.

(36) van de Krol, R.; Grätzel, M. *Photoelectrochemical Hydrogen Production*; *Electronic Materials: Science and Technology*; Springer: New York, 2011.

(37) Dill, R. D.; Joshi, G.; Thorley, K. J.; Anthony, J. E.; Fluegel, B.; Johnson, J. C.; Reid, O. G. Near-Infrared Absorption Features of Triplet-Pair States Assigned by Photoinduced-Absorption-Detected Magnetic Resonance. *J. Phys. Chem. Lett.* **2023**, *14*, 2387–2394.

(38) Blackburn, J. L.; Zhang, H.; Myers, A. R.; Dunklin, J. R.; Coffey, D. C.; Hirsch, R. N.; Vigil-Fowler, D.; Yun, S. J.; Cho, B. W.; Lee, Y. H.; Miller, E. M.; Rumbles, G.; Reid, O. G. Measuring Photoexcited

Free Charge Carriers in Mono- to Few-Layer Transition-Metal Dichalcogenides with Steady-State Microwave Conductivity. *J. Phys. Chem. Lett.* **2020**, *11*, 99–107.

(39) Neilson, K. M.; Hamtaei, S.; Nassiri Nazif, K.; Carr, J. M.; Rahimishikh, S.; Nitta, F. U.; Brammertz, G.; Blackburn, J. L.; Hadermann, J.; Saraswat, K. C.; Reid, O. G.; Vermang, B.; Daus, A.; Pop, E. Toward Mass Production of Transition Metal Dichalcogenide Solar Cells: Scalable Growth of Photovoltaic-Grade Multilayer WSe₂ by Tungsten Selenization. *ACS Nano* **2024**, *18*, 24819–24828.

(40) Tamai, N.; Miyasaka, H. Ultrafast Dynamics of Photochromic Systems. *Chem. Rev.* **2000**, *100*, 1875–1890.

(41) Wen, G.; Zou, X.; Hu, R.; Peng, J.; Chen, Z.; He, X.; Dong, G.; Zhang, W. Ground- and excited-state characteristics in photovoltaic polymer N2200. *RSC Adv.* **2021**, *11*, 20191–20199.

(42) Pankow, R. M.; Harbuzaru, A.; Zheng, D.; Kerwin, B.; Forti, G.; Duplessis, I. D.; Musolino, B.; Ponce Ortiz, R.; Facchetti, A.; Marks, T. J. Oxidative-Reductive Near-Infrared Electrochromic Switching Enabled by Porous Vertically Stacked Multilayer Devices. *J. Am. Chem. Soc.* **2023**, *145*, 13411–13419.

(43) Gish, M. K.; et al. The Excited-State Lifetime of Poly(NDI2OD-T2) Is Intrinsically Short. *J. Phys. Chem. C* **2024**, *128*, 6392–6400.

(44) Earley, J. D.; Zieleniewska, A.; Ripberger, H. H.; Shin, N. Y.; Lazorski, M. S.; Mast, Z. J.; Sayre, H. J.; McCusker, J. K.; Scholes, G. D.; Knowles, R. R.; Reid, O. G.; Rumbles, G. Ion-pair reorganization regulates reactivity in photoredox catalysts. *Nat. Chem.* **2022**, *14*, 746–753.

(45) Carr, J. M.; Allen, T. G.; Larson, B. W.; Davydenko, I. G.; Dasari, R. R.; Barlow, S.; Marder, S. R.; Reid, O. G.; Rumbles, G. Short and long-range electron transfer compete to determine free-charge yield in organic semiconductors. *Materials Horizons* **2022**, *9*, 312–324.

(46) Pace, N. A.; Clikeman, T. T.; Strauss, S. H.; Boltalina, O. V.; Johnson, J. C.; Rumbles, G.; Reid, O. G. Triplet Excitons in Pentacene Are Intrinsically Difficult to Dissociate via Charge Transfer. *J. Phys. Chem. C* **2020**, *124*, 26153–26164.

(47) Hoofman, R. J. O. M.; de Haas, M. P.; Siebbeles, L. D. A.; Warman, J. M. Highly mobile electrons and holes on isolated chains of the semiconducting polymer poly(phenylene vinylene). *Nature* **1998**, *392*, 54–56.

(48) Grozema, F. C.; Siebbeles, L. D. A. Charge Mobilities in Conjugated Polymers Measured by Pulse Radiolysis Time-Resolved Microwave Conductivity: From Single Chains to Solids. *J. Phys. Chem. Lett.* **2011**, *2*, 2951–2958.

(49) Prins, P.; Grozema, F. C.; Schins, J. M.; Savenije, T. J.; Patil, S.; Scherf, U.; Siebbeles, L. D. A. Effect of intermolecular disorder on the intrachain charge transport in ladder-type poly(*p*-phenylenes). *Phys. Rev. B* **2006**, *73*, 045204.

(50) Bird, M. J.; Reid, O. G.; Cook, A. R.; Asaoka, S.; Shibano, Y.; Imahori, H.; Rumbles, G.; Miller, J. R. Mobility of Holes in Oligo- and Polyfluorenes of Defined Lengths. *J. Phys. Chem. C* **2014**, *118*, 6100–6109.

(51) Anderson, M. A.; Larson, B. W.; Ratcliff, E. L. A Multi-modal Approach to Understanding Degradation of Organic Photovoltaic Materials. *ACS Appl. Mater. Interfaces* **2021**, *13*, 44641–44655.

(52) Li, J.; Xu, Q.; Luo, X.; Nie, T.; Wang, M.; She, Y.; Guo, L. Size Effects on Bubble Dynamics during Photoelectrochemical Water Splitting. *ACS Nano* **2025**, *19*, 8200–8211.

(53) Lu, X.; Yadav, D.; He, B.; Zhou, Y.; Zhou, L.; Zeng, Z.; Ma, L.; Jing, D. Unveiling micro- and nanoscale bubble dynamics for enhanced electrochemical water splitting. *Adv. Colloid Interface Sci.* **2025**, *343*, 103544.

(54) Lu, X.; Yadav, D.; Liu, J.; Zeng, Z.; Ma, L.; Jing, D. How dual hydrogen bubble evolution inhibits electrolytic performance. *J. Power Sources* **2025**, *632*, 236356.